Separation Science and Technology
Publication details, including instructions for authors and subscription information:
http://www.informaworld.com/smpp/title~content=t713708471

Theoretical Analysis of a Magnetic Separator Device for Ex-Vivo Blood Detoxification

Haitao Chen[ab]; Armin D. Ebner[c]; James A. Ritter[c]; Michael D. Kaminski[d]; Axel J. Rosengart[e]
[a] Department of Biomedical Engineering, Illinois Institute of Technology, Chicago, IL [b] Department of Neurology, The University of Chicago Medical Center, Chicago, IL [c] Department of Chemical Engineering, University of South Carolina, Columbia, SC [d] Chemical Engineering Division, Argonne National Laboratory, Argonne, IL [e] Departments of Neurology and Surgery (Neurosurgery), The University of Chicago Medical Center, Chicago, IL, USA

To cite this Article Chen, Haitao , Ebner, Armin D. , Ritter, James A. , Kaminski, Michael D. and Rosengart, Axel J.(2008) 'Theoretical Analysis of a Magnetic Separator Device for Ex-Vivo Blood Detoxification', Separation Science and Technology, 43: 5, 996 — 1020
To link to this Article: DOI: 10.1080/01496390801910609
URL: http://dx.doi.org/10.1080/01496390801910609

Separation Science and Technology, 43: 996–1020, 2008

ISSN 0149-6395 print/1520-5754 online
DOI: 10.1080/01496390801910609

Theoretical Analysis of a Magnetic Separator Device for Ex-Vivo Blood Detoxification

Haitao Chen,[1,5] Armin D. Ebner,[2] James A. Ritter,[2] Michael D. Kaminski,[3] and Axel J. Rosengart[4]

[1]Department of Biomedical Engineering, Illinois Institute of Technology, Chicago, IL
[2]Department of Chemical Engineering, University of South Carolina, Columbia, SC
[3]Chemical Engineering Division, Argonne National Laboratory, Argonne, IL
[4]Departments of Neurology and Surgery (Neurosurgery), The University of Chicago Medical Center, Chicago, IL,
[5]Department of Neurology, The University of Chicago Medical Center, Chicago, IL

Abstract: The feasibility of a magnetic separator device for ex-vivo blood detoxification was studied. This blood detoxification approach entails administering functionalized magnetic microspheres (FMMSs) into a patient's body by transdermal injection to capture and remove toxins from the blood using highly specific receptors attached to the surface of the FMMSs. These toxin-loaded FMMSs are then removed from the body using extracorporeal blood circulation through a specially designed magnetic separator, based on high gradient magnetic separation principles. The performance of the magnetic separator, in terms of its collection efficiency (CE) of the FMMSs, was evaluated theoretically using a streamline analysis of a 2-D model. The effects of blood velocity (1 to 20 cm/s), magnetic field strength (0.1 to 2.0 T), wire size (0.125 to 2.0 mm in radii), separator unit size at a fixed ratio of tube to wire diameter of one, tube length (2.0 to 20 cm), wire material (nickel, SS 430 and wairauite), and magnetic material comprising the FMMSs (iron, typical

Received 15 August 2007, Accepted 23 December 2007
Address correspondence to Axel J. Rosengart, Departments of Neurology and Surgery (Neurosurgery), The University of Chicago Medical Center, Chicago, IL 60637, USA. E-mail: arosenga@neurology.bsd.uchicago.edu

magnetite and weaker magnetite) on the CE were evaluated. Provided that the blood velocity was below 2 cm/s, CEs >80% could be attained under reasonable conditions, like when using FMMSs 400 nm in diameter and containing 60 wt% magnetite in a magnetic field of 0.5 T using a magnetic separator with 0.5 mm radii wire (at a fixed ratio of tube to wire diameter of close to one) that was 10 cm in length (same as the tube) and made of SS 430. CEs of between 30% and 80% could also be attained at blood velocities up to 20 cm/s without compromising the magnetic separator design. The magnetic separator performance improved by reducing the size of the unit with tubes and wires of equal radii, increasing the applied magnetic field strength, utilizing magnetic materials with the highest magnetizations, and increasing the length of the unit. Overall, the results from this study delineated the physically realistic conditions that make ex vivo blood detoxification possible with this magnetic separator device.

Keywords: Magnetic separator, defoxification, magnetic microspheres, magnetic separator

INTRODUCTION

In recent years, interest in functionalized magnetic microspheres (FMMSs) has been growing in a number of diverse areas, mainly to exploit their magnetic character. FMMSs are spherically shaped polymers comprised of an inner core that contains well-dispersed superparamagnetic nanoparticles and an outer layer that is functionalized with biochemical receptors (e.g., antibodies) that selectively bind to specific molecules (e.g., antigens). FMMSs are currently being investigated for use in detection systems (1–9), biomolecule and cell separations (10–20), cell sorting (5, 7, 9, 21, 22), hyperthermia treatment (23–25), controlled drug delivery (26), and magnetically stabilized fluidized beds (27, 28). FMMSs are also being investigated for use in the detoxification of patients that have become internally contaminated (e.g., by ingestion or inhalation) with biological, chemical, and/or radioactive toxins (29), where success of the treatment depends on the ability to rapidly and effectively remove these toxins from the patient's body.

For radioactive contamination, for example, current treatment strategies, which generally consist of chelator drug therapies and supportive medical care, are quite inadequate, as they depend ultimately on the body's slow and natural means of excretion. Furthermore, most of these approaches can achieve only modest reductions in the biological half-life of a few selected radionuclides (30–32). However, FMMSs, when utilized with a magnetic separator, offer a different approach for the rapid and effective removal of a variety of toxins from the body (29).

This approach for the magnetic detoxification of blood consists of two steps (29) and involves two well-developed technologies. In the first step, the FMMSs are administered into the patient's body by transdermal injection to capture and remove most, if not all, of the toxins from the blood in the circulatory system. The capture of toxins is realized through

selective chemical reactions with highly specific receptors, e.g., radionuclide chelating agents or monoclonal antibodies, attached to the surface of the FMMSs. In the second step, the toxin-loaded FMMSs are removed from the body using the magnetic separator, which is based on combining two established technologies. The first technology is associated with the high gradient magnetic separation (HGMS) technique, which has many applications in the treatment of biological (1–22, 33–37) and industrial fluids (38–44), and is even being utilized with microfluidic devices (45–48). The second technology is associated with the extracorporeal blood circulation technique, where blood is temporarily removed from the body, treated and then immediately returned to the body. This technique is commonly used in hemodialysis (49–51).

The magnetic separator utilizes a dual-lumen needle for arterial or venous access through the skin to provide extracorporeal blood flow through a short segment of a catheter tube. The blood leaving the body flows through this dual-lumen needle, the catheter tube and into an array of small tubes with ferromagnetic wires placed between each of them. The entire array of tubes and wires is immersed in a magnetic field that causes the FMMSs to be deflected toward the wires and collected on the walls of the tubes. The magnetically detoxified blood then flows out of this array through another section of the catheter tube, then through the dual-lumen needle, and finally back into the body.

The objective of this study is to determine the feasibility of just the magnetic separator device for ex-vivo removal of FMMSs from blood. The performance of this magnetic separator is evaluated theoretically using a streamline analysis of a 2-D model that is solved with the aid of COMSOL Multiphysics^{TM} (52, 53). The effect of several parameters on the ability of this magnetic separator to collect FMMSs is investigated, including the blood velocity, magnetic field strength, magnetic separator wire size and material, magnetic separator unit size at a fixed ratio of tube to wire diameter of unity, tube length, and FMMS magnetic material. The results from this theoretical feasibility study delineate the physically realistic conditions that make *ex vivo* blood detoxification possible with the magnetic separator device.

MAGNETIC SEPARATOR

Figure 1 shows the magnetic separator device in operation, as well as two different views of its internal layout of tubes and wires. Figure 1a shows the portable magnetic separator connected to the vasculature through an artery or vein of a patient's arm using, for example, the dual-lumen needle and tubing. The FMMSs in the blood access the magnetic separator through this tube and become retained within the unit via HGMS principles. The detoxified blood, which is now free of the FMMSs, is then returned back to the blood

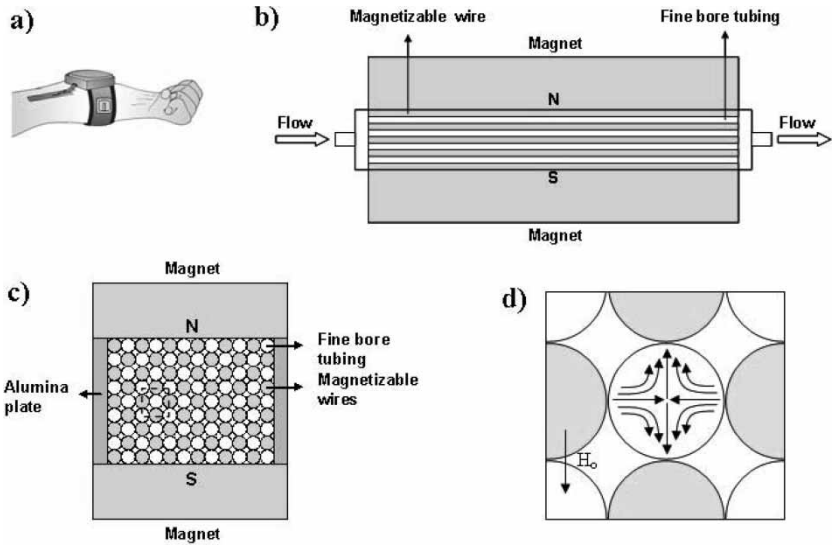

Figure 1. a) One of many possible modes of operation of a magnetic separator device designed for *ex vivo* blood detoxification; b) Schematic of one of many possible magnetizable wire and capillary tube array configurations positioned between two rectangular permanent magnets inside the magnetic separator; c) Cross-sectional view of the magnetizable wire and capillary tube array and permanent magnet configuration shown in Figure 1b; d) Schematic of the FMMS trajectories inside one of the capillary tubes in the magnetic separator, depicting the attractive and repulsive zones generated inside the tube as result of the interaction of the FMMSs with the four surrounding magnetized wires exposed to magnetic field H_o oriented as shown.

stream through a tube that leads to the same dual-lumen needle. Figure 1b shows the parallel array of alternating magnetizable wires (dark) and capillary tubes (white) inside the unit that are immersed in a homogeneous magnetic field produced by two rectangular permanent magnets positioned on each side of the array in an axial configuration. In this configuration, the magnetic field is perpendicular to both the magnetizable wires and the capillary tubes.

Each capillary tube is surrounded by four ferromagnetic wires, except for the few capillary tubes located at the periphery of the array. This arrangement is shown in a cross-sectional view of the array in Fig. 1c and in an expanded view in Fig. 1d. The axes of the two wires lying above and below the capillary tube lie in the plane of the magnetic field; thus, they have their attractive polarized sides facing the capillary tube. The axes of the two wires lying to the left and right of the capillary tube lie in the plane that is perpendicular to the magnetic field. Thus, they have their repulsive polarized sides facing the capillary tube. Typical magnetic field lines depicting this situation inside a capillary tube are shown in Fig. 1d.

As the FMMSs in the blood travel through the capillary tube, the energized ferromagnetic wires exert a magnetic force on them by virtue of the HGMS principle. This magnetic force must overcome the hydrodynamic force to deflect the FMMSs out of their hydrodynamic streamline trajectory and direct them toward the wall of the tube. When this happens, the FMMSs necessarily move toward one of the two wires with its attractive polarized side facing the capillary tube, while simultaneously moving away from the other two wires with their repulsive polarized sides facing the capillary tube (Fig. 1d). Provided that the magnetic force is sufficiently strong, some (possibly all) of the FMMSs become retained along the wall of the capillary tube that is adjacent to the attractive polarized wires, thereby magnetically capturing them within the device.

MODEL DEVELOPMENT

The performance of the magnetic separator shown in Fig. 1 is evaluated using a simplified approach based on the 2-D control volume (CV) shown in Fig. 2. The 2-D CV represents the bisecting plane of the simplified unit shown in

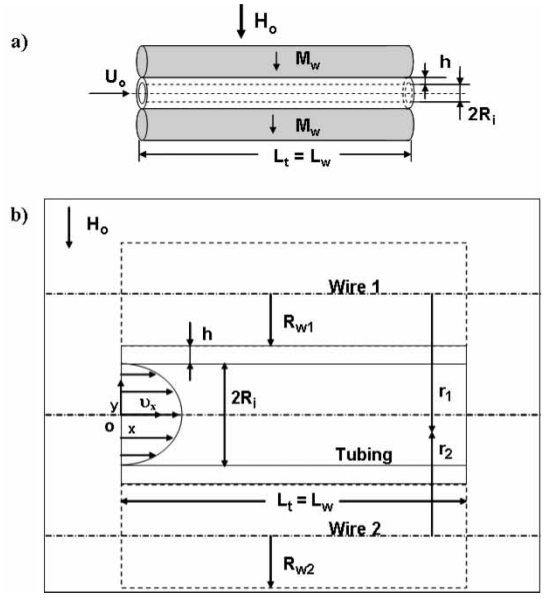

Figure 2. a) Schematic diagram of a simplified representation of the multi-tube and multi-wire array shown in Figure 1, depicting a single tube positioned between two magnetizable wires; b) Schematic diagram of the 2-D control volume (CV) developed for modeling the collection efficiency of the FMMSs of the two wires, single tube configuration.

Fig. 2a, which consists of a single capillary tube placed in between two ferromagnetic wires with their attractive magnetically polarized sides facing the tube. Thus, the performance of the multi-tube and multi-wire magnetic separator in Fig. 1 is evaluated in terms of the dynamics observed within this bisecting plane that contains the axes of the tube and wires and the homogeneous magnetic field placed perpendicular to these axes. The rationale behind this simplification is given later.

The magnetizable wires with radius R_w and length L_w are represented by the area embraced by the dashed lines and placed above and below the capillary tube of radius R_i, length L_t ($=L_w$), and wall thickness h. The blood travels through the capillary tube from left to right with average velocity U_o while transporting a homogeneous dispersion of FMMSs. As indicated earlier, the wires are subjected to a homogeneous magnetic field of strength H_o positioned perpendicular to the blood flow and wires in an axial configuration. As the blood travels through the capillary tube the FMMSs become magnetically diverted towards the capillary walls by the magnetic field of the wires. A FMMS is assumed to be captured when its trajectory makes contact with the wall of the tube. The goal is to evaluate the performance of this 2-D CV by analyzing the fraction of trajectories of the FMMSs that reach the capillary tube wall before leaving the CV as they travel through this 2-D representation under the influence of both hydrodynamic and magnetic forces.

The FMMS trajectories are determined through a streamline function analysis. Like in previous work (52, 53), the gist of this model is based on a force balance over a single FMMS, which allows for explicit expressions of its component velocities to be obtained. The streamline function that is derived from these component velocities ultimately represents the trajectories of the FMMSs as they travel through the tube. To obtain these explicit expressions of the component velocities, the model only accounts for the hydrodynamic and magnetic forces acting upon a single FMMS. Other forces such as inertial (54), gravitational (generally less than $1/1000$ of magnetic force), wall effects and interparticle interactions are neglected for now. It is worth noting that the model developed here differs from those developed previously (52, 53), in terms of how both the fluid flow and magnetic fields within the separator (i.e., tube) are determined. In this case, rather than numerically solving the Navier Stokes and Maxwell equations to respectively evaluate fluid flow and magnetic fields (52, 53), the model utilizes convenient analytical expressions for the same purpose, as explained below.

In summary, the model consists of three parts. First, the hydrodynamic force upon the FMMS is determined using Stokes relationship and by assuming a parabolic flow regime with an average velocity U_o for the blood flow within the bisecting plane of the capillary tube. Second, the magnetic force upon the FMMS is determined using known analytical expressions that describe the magnetic field around magnetizable wires under the

influence of a homogenous magnetic field H_o. The expressions that describe these two forces are then formulated into a system of two equations that represent the x and y components of a momentum balance carried out on a single FMMS of radius R_p. Because inertial terms are neglected, these two expressions lead to explicit analytical expressions for the component velocities of a single FMMS, i.e., $v_{p,x}$ and $v_{p,y}$. Third, Comsol Multiphysics™ is then used to numerically solve the corresponding stream functions for the flow field defined and determined from the components of the velocity of the FMMS. Once the trajectories of the FMMSs are resolved within the CV, they are used to evaluate the retention or collection efficiency of the FMMSs, as readily indicated by a visual inspection of the collective paths taken by the trajectories.

For part one of the model, the hydrodynamic force upon a FMMS is determined by assuming that the fluid dynamics in the tube are described by a parabolic flow profile obtained by solving analytically the 2-D Navier-Stokes equation for a steady incompressible Newtonian fluid moving inside a tube. The fluid velocity v is thus described by

$$v = (v_x, v_y) = \left(2.0\left(1 - \left(\frac{y}{R_i}\right)^2\right)U_o, 0\right) \tag{1}$$

where v_x and v_y are the components of the fluid velocity, and R_i is the tube inner radius. According to Stokes equation, the corresponding hydrodynamic force (i.e., the drag force, F_d) on an FMMS becomes:

$$F_d = 6\pi\eta R_p(v - v_p) \tag{2}$$

where η is the fluid viscosity and v_p is the velocity of a FMMS.

In the second part of the model, the magnetic force exerted by the wires on a FMMS located within the bisecting plane is resolved by first determining the magnetic field H created by the two wires under a homogenous magnetic field H_o. For any point within the bisecting plane between the two parallel magnetized wires, this magnetic field is given by the following analytical expression:

$$H = H_o + \frac{1}{2}M_w\left(\frac{R_{w1}^2}{r_1^2} + \frac{R_{w2}^2}{r_2^2}\right) \tag{3}$$

M_w is the magnetization of the wires. R_{w1} and R_{w2} are the radii of wire 1 and wire 2, respectively. r_1 and r_2 represent the absolute distance from a given point from the bisecting plane (i.e., from a FMMS located in it) to the axes of wires 1 and 2, respectively. It is assumed that R_{w1} and R_{w2} are identical and that the wires are in contact with the capillary tube. Assuming that the magnetic susceptibility is large enough and that demagnetization effects govern the internal magnetic field within the wires, M_w and H_o are related according to

$$|M_w| = \min(2|H_o|, M_{w,s}) \tag{4}$$

where $M_{w,s}$ is the magnetization of the wire at saturation. The expressions in Eqs. (3) and (4) are then used to evaluate the magnetic force (F_m) upon the FMMS according to:

$$F_m = \Omega_{fm}\omega_{fm,p}V_p\mu_o\nabla(M_{fm}\cdot H) \tag{5}$$

where V_p is the volume of the FMMS, μ_o is the magnetic permeability of vacuum, and $\omega_{fm,p}$ is the volume fraction of the ferromagnetic material with magnetization M_{fm} inside the FMMS. $\omega_{fm,p}$ is related to its weight fraction $x_{fm,p}$ through:

$$\omega_{fm,p} = \frac{x_{fm,p}}{x_{fm,p} + (1 - x_{fm,p})(\rho_{fm,p})/(\rho_{pol,p})} \tag{6}$$

where $\rho_{fm,p}$ is the density of the ferromagnetic material in the FMMS and $\rho_{pol,p}$ is the density of the polymer material comprising the FMMS. Ω_{fm} is a continuous function that approaches unity when the magnetization of the ferromagnetic material approaches saturation and one-half when it approaches a linear behavior at low magnetic fields. Furthermore, Ω_{fm} is such that Eq. (5) becomes

$$\mathbf{F_m} = \frac{1}{2}\omega_{fm,p}V_p\mu_o\frac{M_{fm}}{H}\nabla(\mathbf{H}\cdot\mathbf{H}) \tag{7}$$

where M_{fm} and H are the magnitudes of M_{fm} and H, respectively.

Because the ferromagnetic material in each FMMS is assumed to consist of fully dispersed, single domain, spherical, magnetic particles of radius R_{sdp}, the relationship between the magnetization M_{fm} and H is assumed to follow Langevin's formulation:

$$M_{fm} = M_{fm,s}\left[\coth\left(\frac{\mu_o M_{fm,s}V_{sdp}(H - (1/3)\omega_{fm,p}M_{fm})}{k_bT}\right) - \frac{k_bT}{\mu_o M_{fm,s}V_{sdp}(H - (1/3)\omega_{fm,p}M_{fm})}\right] \tag{8}$$

where $M_{fm,s}$ is the saturation magnetization of the ferromagnetic material inside the FMMS, V_{sdp} is the volume of a single magnetic particle inside the FMMS, k_b is the Boltzman constant, and T is the absolute temperature. The term, $1/3\omega_{fm,p}M_{fm}$, accounts for the demagnetization field due to the FMMS as a whole. For simplicity, however, this term is neglected, mainly due to the small volume fraction $\omega_{fm,p}$ occupied by the ferromagnetic particles inside a FMMS.

The last step of the model consists of determining the streamlines that represent the trajectories of the FMMS along the CV of Fig. 2b under both magnetic and hydrodynamic drag forces. This is realized by first obtaining explicit expressions for the component velocities of an FMMS, v_p, after the application of a force balance upon a single FMMS and considering only the magnetic and hydrodynamic forces expressed in Eqs. (2) and (7). The

following explicit expression is obtained for υ_p:

$$\upsilon_p = \upsilon + \frac{1}{9}\frac{\mu_o R_p^2 \omega_{fm}}{\eta}\frac{M_{fm}}{H}\nabla(\mathrm{H}\cdot\mathrm{H}) \tag{9}$$

The stream function ψ is then obtained from the component velocities of the FMMS through the following well known definitions (55):

$$\frac{\partial\psi}{\partial y} = -\upsilon_{p,x} \quad \frac{\partial\psi}{\partial x} = \upsilon_{p,y} \tag{10}$$

which are numerically solved using the stream function analysis incorporated in Comsol Multiphysics™. It is important to indicate that because of the nature of the streamline function the boundary conditions used in solving Eq. (10) are completely arbitrary. Once the solution of the stream function is obtained, Comsol Multiphysics™ provides a clear visualization of the corresponding streamlines, with each representing the trajectory of a single FMMS as it travels through the CV under the influence of both magnetic and hydrodynamic forces. The performance of this system is finally determined by its collection efficiency (CE), which is qualitatively defined as the fraction of FMMS trajectories that enter homogeneously from the left side of the CV and become attracted to the wires, as indicated by the fraction of trajectories that end up touching the wall of the tube. A quantitative definition of CE is given later.

RESULTS AND DISCUSSION

The base conditions chosen for this modeling study are considered to be reasonable for the design of an ex vivo magnetic separator for blood detoxification. They coarsely take into account the physics behind maximizing the magnetic force on the FMMS, as well as the physiology behind minimizing the energy required to pump the blood through the device, which ideally comes from the pumping action of the heart. They also take into consideration some of the key requirements of this magnetic blood detoxification approach (29), which include highly specific FMMSs that are biocompatible and no more than about 2.0 to 3.0 μm in diameter to assure free circulation within the body; a magnetic field that is produced by a permanent magnet, such as a NdFeB magnet, to eliminate energy requirements; a tube that is biocompatible with thin walls to maximize magnetic field strength; wires that are ferromagnetic and of small diameter; a separation capacity that is capable of processing the total volume of blood in the body within a short period of time, e.g., four to six liters in 30 to 60 min; a capture efficiency that is greater than about 80% for one pass through the magnetic separator; and weight and volume that make it portable and easy to use in the field.

Based on preliminary calculations associated with the physics and physiology of the magnetic separator device, the base case conditions of this modeling study turned out to be the following. The tube has an outer diameter of 1.0 mm, an inner diameter of 0.75 mm and a length of 100 mm. The wires are made of SS 430 with a diameter of 1.0 mm and a length of 100 mm. The FMMSs have a diameter of 400 nm and contain 60 wt% magnetite. A homogenous magnetic field of 0.5 T is applied, and the blood velocity through the tube is 5.0 cm/s. These base case conditions lead to a magnetic separator with 126 tubes, when assuming that 5 liters of blood is processed in 30 min. This is considered to be a reasonable number of tubes.

The parametric study that is carried out systematically varies some of these base case parameters in the model, while keeping all the other parameters fixed at the base case conditions unless otherwise noted. The ranges of these parameters are listed in Table 1. Table 2 provides other physical and magnetic properties required in this modeling study. It is noteworthy that at the extreme ranges of tube sizes and fluid velocities through the tube (Table 1) the magnetic separator requires as few as 10 tubes and as many as 4,670 tubes to process 4 to 6 iters of blood in 30 min. Only half the number of tubes is required if the processing time is extended to 60 min. This range of parameters covers a sufficient number of magnetic separator tube and wire array designs and sizes, with dimensions even approaching the range of microfluidic devices (45–48).

Table 1. Values and ranges of the parameters used in the model[a]

Parameters	Units	Values
Fluid density, ρ	kg/m^3	1000
Fluid viscosity, η	kg/(m s)	3.0×10^{-3}
Fluid temperature, T	K	298.15
Mean fluid velocity, U_o	cm/s	1.0 – 20.0, 5.0
Tube inner radius, R_i	mm	0.150, 0.225, 0.375, 0.600
Tube outer radius, R_o	mm	0.200, 0.300, 0.500, 0.800
Tube wall thickness, h	mm	0.050, 0.075, 0.125, 0.200
Tube length, L_t	mm	20, 50, 100, 200
FMMS radius, R_p	nm	200
FMMS material[b]		weaker magnetite, magnetite, Fe
FMMS radius, R_{fm}	nm	5
FMMS ferromagnetic mass fraction, $x_{fm,p}$		0.6
FMMS polymer density, ρ_{pol}	kg/m^3	950
Wire material[b]		Ni, SS 430, wairauite
Wire radius, R_w	mm	0.125, 0.25, 0.5, 1, 2
Wire length, L_w	mm	20, 50, 100, 200
Magnetic field flux density, $\mu_o H_o$	T	0.1–2.0, 0.5

[a]Base case conditions underlined.
[b]properties indicated in Table 2.

Table 2. Physical properties of ferromagnetic materials used in the model

Material	$\rho_{fm,p}$ or ρ_w (kg/m^3)	$M_{w,s}$ or $M_{fm,s}$ (kA/m)
Iron[a]	7850	1735
Magnetite[a]	5050	450
Weaker Magnetite[a]	5050	150
Stainless steel 430[b]	—	1365
Nickel[b]	—	490
Wairauite (CoFe)[b]	—	1922

[a]Magnetic material in the FMMS.
[b]magnetic material of the wire.

One of the most important considerations in the design of the magnetic separator is the arrangement of the alternating array of tubes and wires inside of it. The array in Fig. 1 conceivably minimizes the fluid (blood) velocity through the capillary tube while maximizing the magnetic force density (F_{md}) (56), with both giving rise to larger collection efficiencies of the FMMSs. An important question to ask is: What magnetic force density can be expected from such a design? Typical simulation results that address this issue are shown in Fig. 3, which map the 2-D magnetic force density field (i.e., $F_{md} = 0.5\,V\nabla\,(H \cdot H)$) through a cross-sectional area of the magnetic dialyzer shown in Fig. 1. The mathematical analysis underlying these simulations of the F_{md} are based on the determination of the magnetic field H using Maxwell's equations and a procedure described elsewhere (52, 53); they are not described here, because they cannot be used to evaluate the collection efficiencies of this system, which is the primary goal of this work through the much simplified mathematical analysis of the two wire, single capillary tube system (Fig. 2).

The results in Fig. 3 show that a F_{md} on the order of $1 \times 10^9\ N/m^3$ can be expected from such a design, which is large enough to foster significant collection of the FMMSs, as shown later. These simulations also show that very broad attractive zones exist within both the top and bottom regions of the tube, with the best localized collection regions corresponding to the vertical plane indicated by the solid white line in Fig. 3a that vertically passes through the magnetic poles of the wires and symmetrically bisects the tube. Because these are the regions where the maximum FMMS collection is expected to occur inside the tube, this is also the planar region selected for obtaining the analytical expression for H Eq. (3), a critical simplifying assumption in this analysis that cannot be overstated.

An approximation of the magnitude of the magnetic field that can be generated in such a device (even above H_o), and its variation within the tube (a direct indication of the possible gradients that can be generated) is

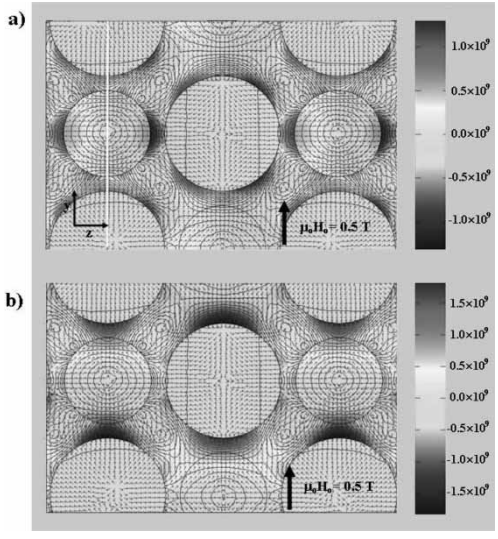

Figure 3. Results obtained from COMSOL Multiphysics^{TM} showing simulations of the 2-D magnetic force density field (i.e., $F_{md} = 0.5\nabla(\mathrm{H} \cdot \mathrm{H})$) through a cross sectional area of the magnetic separator array configuration shown in Figure 1. The arrows and contour lines respectively indicate the direction and intensity of the magnetic field density, with darker regions indicating higher intensities. Red (i.e., positive) and blue (i.e., negative) colorations indicate that the a) $\times$ and b) y components of the magnetic field point in the positive and negative directions of the coordinate system, respectively. The white line in (a) indicates the bisecting plane upon which Eq. 2 for H is based. The large circles are the wires and the small circles are the tubes, both with the same outside diameter. Conditions: $\mu_o H_o = 0.5$ T, $R_i = 0.375$ mm, $h = 0.125$ mm, $L_t = L_w = 100$ mm, SS 430 wire, and $R_w = 0.5$ mm.

shown in Figure 4 for different wire sizes (R_w). These results were obtained from Eq. (3), which describes the variation of the magnetic field in the y-direction according to the simplified 2-D CV displayed in Fig. 2b. Clearly, the magnitude of the magnetic field and its gradients both depend very strongly on the wire diameter, with larger wires giving rise to larger overall magnetic fields but smaller more dispersed gradients. The smallest wire (0.125 mm) produced the largest magnetic field gradient near the wires. However, the magnetic field far from the wires and close to the center of the tube becomes more homogeneous and quite small at about 0.6 T. In contrast, the magnitude of the magnetic field generated from the largest wire (2.0 mm) is much higher at around 1.2 T, with its rather shallow gradients persisting well into the center of the tube. In either case, the results cannot be used to elucidate whether the magnetic forces are smaller and shorter ranged for the smaller wire due to the smaller magnitudes of the magnetic fields and its diminished gradients, or whether the magnetic forces are larger and longer ranged for the larger wire due to the larger

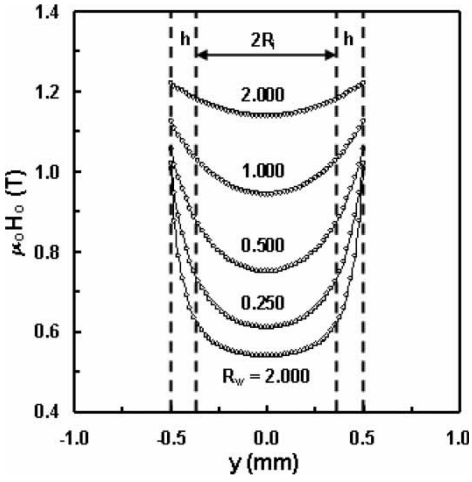

Figure 4. Effect of the wire radius (R_w) on the variation of the magnetic field intensity ($\mu_o H_o$) within the tube when placed between the two parallel and identical wires. Conditions: $\mu_o H_o = 0.5$ T, $R_i = 0.375$ mm, $h = 0.125$ mm, $L_t = L_w = 100$ mm, SS 430 wire, $R_p = 200$ nm, and $x_{fm,p} = 0.6$ with the FMMSs comprised of typical magnetite.

magnitudes of the magnetic fields and its shallow but continual gradients. This important design issue is addressed below via the parametric study that reveals the effect of the wire size, as well as the effects of other parameters, on the collection efficiency of the FMMSs.

Typical simulation results of the simplified 2-D representation of the magnetic separator depicted in Fig. 2b are displayed in Fig. 5. The thick white lines indicate the trajectories of the last FMMS captured by the separator, which are determined by visual inspection. The collection efficiency (CE) defined earlier, but only qualitatively in terms of the FMMS trajectories, is defined quantitatively in terms of these thick white lines according to the following equation

$$CE(\%) = 100\frac{R_i - y_{\max}}{R_i} \tag{11}$$

where $y_{\max}$ is the y-coordinate (evaluated at $x = 0$ in Fig. 2) of the last FMMS streamline captured in the top half of the separator. The resulting CE for these base case conditions is 59%. Note that Eq. (11) assumes the FMMSs (modeled as point masses) enter the tube distributed evenly along the y-axis at the inlet of the CV. This assumption ignores the fact that the FMMSs close to the wall of the tube may tend to move toward the center of the tube due to lift forces and other wall effects, which are not accounted for in this simplified analysis.

The effect of the wire size (R_w) on the capture efficiency (CE) of the FMMSs as a function of U_o is shown in Fig. 6a for the base case conditions.

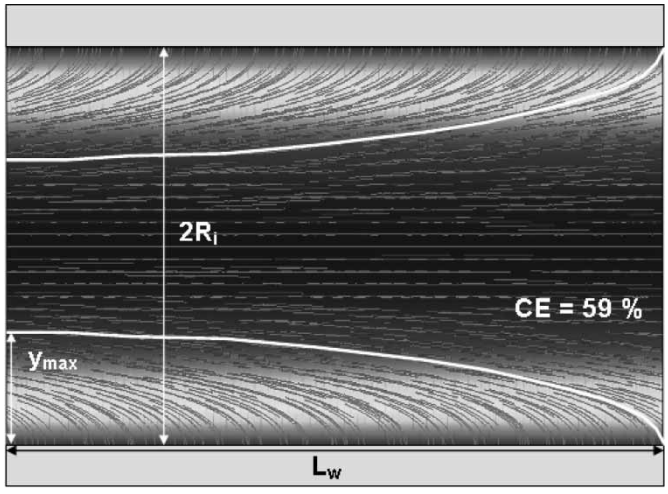

Figure 5. Typical results obtained from COMSOL Multiphysics™ showing simulations of the FMMS streamlines within the simplified 2-D CV depict in Figure 2b. Conditions: $\mu_o H_o = 0.5$ T, $R_i = 0.375$ mm, $h = 0.125$ mm, $L_t = L_w = 100$ mm, SS 430 wire, $R_w = 0.5$ mm, $U_o = 5$ cm/s, $R_p =$ 200 nm, and $x_{fm,p} = 0.6$ with the FMMSs comprised of typical magnetite.

For all R_w, as U_o increases CE decreases rather sharply at low velocities and then more gradually at higher velocities. Moreover, the CEs range from 75% to 93% at $U_o = 1$ cm/s and from 11% to 31% at $U_o = 20$ cm/s, indicating a significant effect of velocity on the CE. Since the magnetic force is being held constant under these conditions, as U_o increases the hydrodynamic force increases resulting in an increasingly larger imbalance in these forces, which manifests as a decreasing CE. Nevertheless, CEs as high as 31% are still attained even for large velocities of 20 cm/s. This somewhat favorable result is a consequence of the fluid flow in the capillary tube having a parabolic velocity profile in the laminar flow regime, which in turn ensures the domination of magnetic forces near the capillary tube wall. Indeed, this result sheds some light on the potential robustness of the design of the magnetic separator for blood detoxification.

In contrast, when these results are plotted with the CE as a function of R_w, as in Fig. 6b, a clear maximum is observed in the CE with increasing R_w, which is quite consistent over the entire range of velocities. The lowest CE is also exhibited by the largest R_w in all cases. These results reveal that an optimum wire radius of around 0.50 mm exists for this set of conditions that is essentially independent of the fluid velocity. In fact, it is quite interesting that at the optimum CE the size of the wires matches quite well with the radius of the capillary tube. Referring to Fig. 4, this result unequivocally illuminates the importance of the interplay between the magnitudes of both the localized magnetic field and the localized magnetic field gradients, with

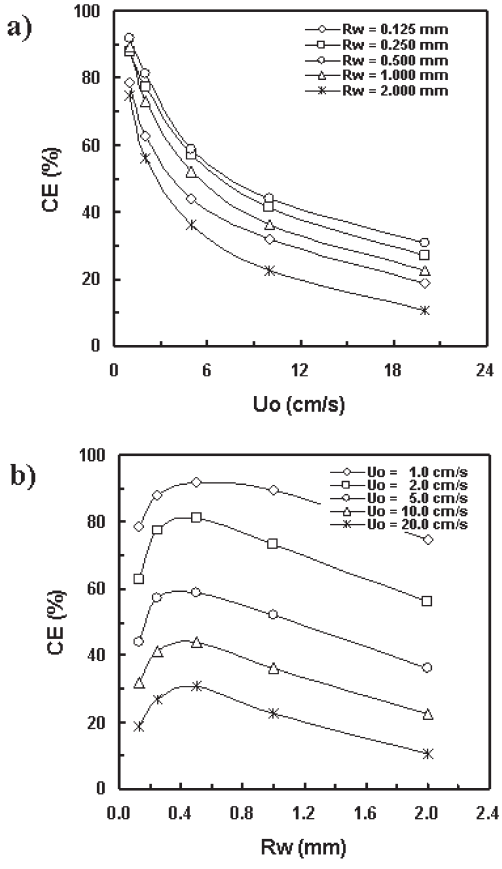

Figure 6. a) Effect of the wire radius (R_w) on the capture efficiency (CE) of the FMMSs with CE plotted as a function of the velocity (U_o). b) Effect of the velocity (U_o) on the capture efficiency (CE) of the FMMSs with CE plotted as a function of the wire radius (R_w). Conditions: $\mu_o H_o = 0.5$ T, $R_i = 0.375$ mm, $h = 0.125$ mm, $L_t = L_w = 100$ mm, SS 430 wire, $R_p = 200$ nm, and $x_{fm,p} = 0.6$ with the FMMSs comprised of typical magnetite.

slightly lower magnitudes in the localized magnetic field and much higher localized magnetic field gradients from the smaller wires combining to produce the larger force and thus larger CE. The results in Fig. 6b thus indicate that the best performance can be expected when the sizes of both the wires and the capillary tubes are identical (i.e., $R_w = R_o$).

This interesting result is further examined in Fig. 7, which displays the effect of the outer capillary tube radius ($R_o = R_i + h$) on the CE of the FMMSs for the base case conditions, while keeping R_o/R_w at the optimum ratio of unity, and while also maintaining $R_i/R_o = 0.75$. The results show the positive effect of reducing the size of the unit on its performance, which is strictly a consequence

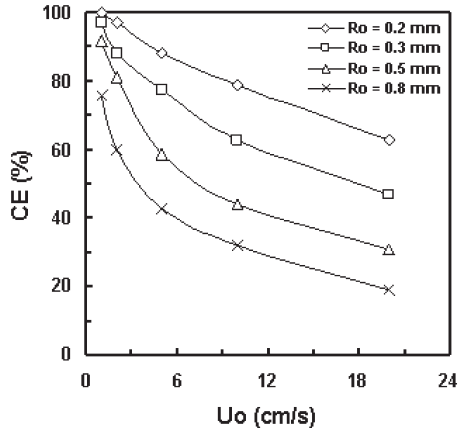

Figure 7. Effect of the capillary tube radius ($R_o = R_i + h$) on the capture efficiency (CE) of the FMMSs with CE plotted as a function of the velocity (U_o). Conditions: $\mu_o H_o = 0.5$ T, $R_o/R_w = 1$, $R_i/R_o = 0.75$, $L_t = L_w = 100$ mm, SS 430 wire, $R_p = 200$ nm, and $x_{fm,p} = 0.6$ with the FMMSs comprised of typical magnetite.

of the HGMS principle. For example, at $U_o = 5$ cm/s, the CE increased from 59% to about 88% when the base case R_o decreased from 0.5 mm to 0.2 mm. This is a significant improvement that matches the results attained at velocities of 2 cm/s or lower in Fig. 6a. It is clear then that the capture efficiency tends to benefit from the miniaturization of the magnetic separator components, to the point where microfluidic devices with microscale or even nanoscale magnetic elements (45–48) may be advantageous. However, keep in mind that the extent of the miniaturization is limited by the size of FMMSs, the number of them that must be removed from the blood, and the shear volume of blood that must be processed for effective blood detoxification.

Figure 8a depicts the effect of the capillary (or wire) tube length ($L_t = L_w$) on the CE of the FMMSs for different U_o and the base case conditions. Because of the longer residence times, the CE improved, as expected, with increasing L_t. Again, significant CEs of 90% and larger can easily be attained with $U_o \leq 2.0$ cm/s and with capillary tubes of reasonable lengths of less than about 10 cm. To attain similar CEs at faster velocities, however, much longer L_t are required, which may not be practical. For example, to achieve CEs of at least 80% at $U_o = 5.0$ cm/s, the unit requires capillary tubes of at 20 cm long, a value perhaps too long for an extracorporal unit.

Intuitively, the results in Fig. 8a should collapse into a single curve when expressing the CE as function of the fluid residence time L/U_o. This relationship is confirmed in Fig. 8b, which simply indicates that the axial and radial movements of the FMMSs are controlled by independent mechanistic processes. Notice, for example, that the momentum balance in Eq. (9)

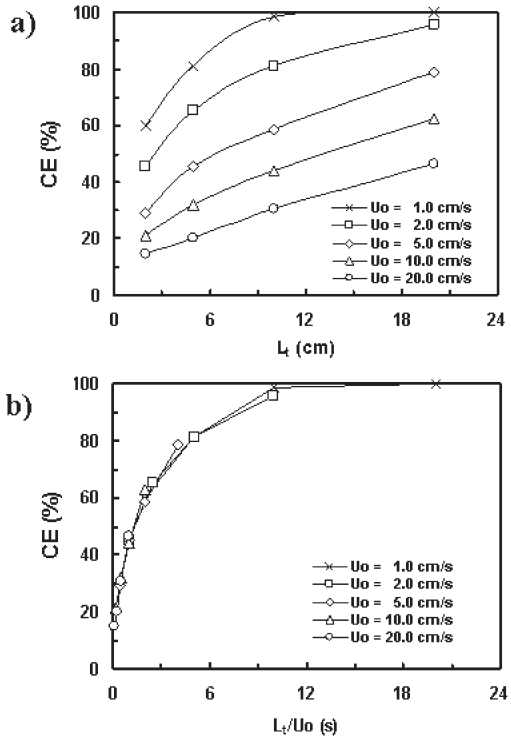

Figure 8. Effect of the tube length (L_t) on the capture efficiency (CE) of the FMMSs with CE plotted as a function of (a) tube length L_t and (b) residence time L_t/U_o for different velocities (U_o). Conditions: $\mu_o H_o = 0.5$ T, $R_i = 0.375$ mm, $h = 0.125$ mm, SS 430 wire, $R_w = 0.5$ mm, $R_p = 200$ nm, and $x_{fm,p} = 0.6$ with the FMMSs comprised of typical magnetite MMS.

implies that the radial movement of a FMMS towards the capillary tube wall should remain unaffected by its axial location or the force it experiences in the axial direction.

The effect of the magnetic material of the wire on the CE of the FMMSs as a function of U_o and $\mu_o H_o$ is shown for the base case conditions in Figs. 9a and 9b, respectively. Three materials are investigated, which, in the order of increasing magnetic character, are nickel, stainless steel (SS) 430, and wairauite (a CoFe alloy). The saturation magnetization of these materials is displayed in Table 2. Nickel, being the weakest magnetic material, exhibited the least effective behavior, with CEs varying from about 84% at $U_o = 1$ cm/s to about 24% at $U_o = 20$ cm/s, as shown in Fig. 9a. SS 430 and wairauite, however, exhibit identical behavior in this figure with CEs of 93% at $U_o = 1$ cm/s and 31% at $U_o = 20$ cm/s, despite their significant differences in magnetic character (i.e, $M_{w,s} = 1365$ and 1922 kA/m, respectively). This apparent paradoxical result, which is predicted by Eq. (4), is simply a

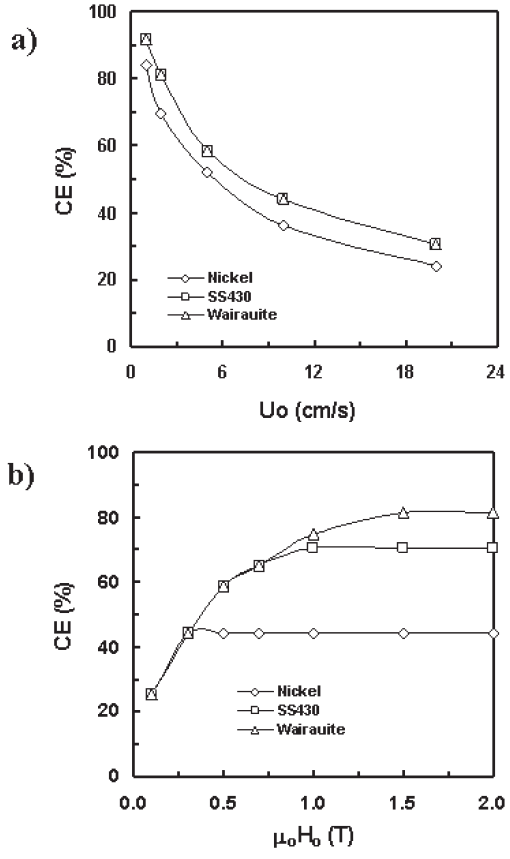

Figure 9. Effect of the wire material on the capture efficiency (CE) of the FMMSs with CE plotted as a function of a) velocity (U_o) and b) applied magnetic field intensity ($\mu_o H_o$). Conditions: $\mu_o H_o = 0.5$ T (a), $U_o = 5$ cm/s (b), $R_i = 0.375$ mm, $h = 0.125$ mm, $L_t = L_w = 100$ mm, $R_w = 0.5$ mm, $R_p = 200$ nm, and $x_{fm,p} = 0.6$ with the FMMSs comprised of typical magnetite.

consequence of both materials being magnetically unsaturated at the applied magnetic field of 0.5 T, a condition satisfied when the applied magnetic field is less than half the magnitude of the saturation magnetizations of both materials. This behavior is due to demagnetization effects, which depend solely on the shape and not the magnetic nature of the magnetized material, control the magnetic behavior of the magnetically unsaturated materials with strong magnetic susceptibilities. This behavior is more clearly depicted in Fig. 9b.

Before reaching a magnetic field of about 0.31 T, which is the saturation condition for Ni ($M_{w,s} = 490$ kA/m), all three materials are magnetically unsaturated and thus they display the same magnetic behavior in Fig. 9b.

Past this point, however, the CE for the saturated nickel remains constant at a value of 44%, while the CEs corresponding to SS 430 and wairauite continue to increase together as one curve until the magnetic field reaches 0.86 T, which is the condition that magnetically saturates the SS 430. Past this magnetic field, the CE for SS 430 remains constant at about 70% while the CE for wairauite continues to increase until it finally reaches magnetic saturation at 1.21 T with a CE of around 80%.

The results just described are significant because they exhibit the extraordinary ability of magnetic materials to display identical behavior in relatively strong magnetic fields despite their significant differences in magnetic character. For example, it takes an appreciable magnetic field of 0.31 T for the CEs obtained with nickel and wairauite to differ even though there is a four-fold difference in the saturation magnetizations of these two metals. Another result that is equally significant is the fact that there is no need to generate a magnetic field inside the magnetic separator unit that is larger than about 1.5 T. At 1.5 T, most ferromagnetic materials of cylindrical shape are already magnetically saturated. This fact alludes to the inherent flexibility of the magnetic separator design for FMMS collection, because of the wide range of soft ferromagnetic materials that are available with saturation magnetizations between those of Ni and wairauite. In this regard, the important role of the magnetic field on the CE of this system cannot be overstated. For example, the results in Fig. 9b show that for certain ferromagnetic materials, the CE can be easily and nearly doubled from 44% to 75% by increasing the applied magnetic field from 0.3 T to about 1.0 T.

Finally, the effect of the magnetic material in the FMMSs on their CE is shown in Figs. 10a and 10b, respectively, as a function of U_o and $\mu_o H_o$, and for the base case conditions. Three materials are evaluated, namely iron and two types of magnetite. The first type of magnetite is a typical magnetite with $M_s = 450\ kA/m$. The second type of magnetite is a hypothetical magnetite with $M_s = 150\ kA/m$, which is just one-third that of typical magnetite. Not surprisingly, iron displays the best CEs. At $U_o = 1.0\ cm/s$, decreasing CEs of 99%, 92%, and 70% are achieved with iron, typical magnetite and weaker magnetite, respectively. In contrast, at 20 cm/s, the respective CEs are 45%, 31%, and 18%. The use of stronger ferromagnetic materials, such as Fe or other equally magnetic metals or alloys, over commonly used iron oxides of weaker magnetic character, like magnetite, is clearly advantageous. For example, in most cases depict in Figs. 10a and 10b, the FMMSs containing Fe display CEs 20% larger than those containing typical magnetite, allowing for the possibility of achieving CEs over 80% at $U_o = 5\ cm/s$. It is noteworthy that unlike the wire materials and model predictions for magnetic particles reported elsewhere (52, 53), these different materials do not exhibit identical behaviors at low magnetic fields. This result is a consequence of the fact that the magnetic particles within the FMMSs are assumed to consist of dispersed single domains. Thus, their magnetic behavior is no

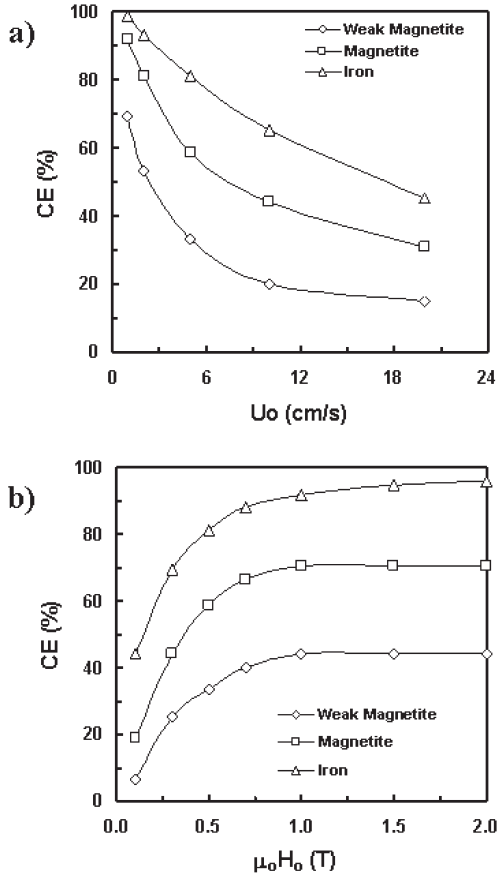

Figure 10. Effect of the magnetic material in the FMMSs on their capture efficiency (CE) with CE plotted as a function of a) velocity (U_o) and b) applied magnetic field intensity ($\mu_o H_o$). Conditions: $\mu_o H_o = 0.5$ T (a), $U_o = 5$ cm/s (b), $R_i = 0.375$ mm, $h = 0.125$ mm, $L_t = L_w = 100$ mm, SS 430 wire, $R_w = 0.5$ mm, $R_p = 200$ nm and $x_{fm,p} = 0.6$.

longer controlled by demagnetization effects as reported earlier (52, 53). Rather, Langevin's relationship in Eq. 8 more appropriately represents their magnetic behavior.

CONCLUSIONS

The objective of this study was to determine the feasibility of a magnetic separator device for the *ex-vivo* detoxification of blood. The notion entails administering functionalized magnetic microspheres (FMMSs) into a

patient's body by transdermal injection to capture and remove toxins from the blood stream using highly specific receptors, e.g., radionuclide chelating agents or monoclonal antibodies, attached to the surface of the FMMSs. These toxin-loaded FMMSs are then removed from the body using extracorporeal blood circulation through a specially designed magnetic separator, based on the high gradient magnetic separation concept.

The magnetic separator device simply uses a dual-lumen needle to puncture an artery or vein to gain access to the previously injected FMMSs in the blood. By the pumping action of the heart, these FMMSs are then transported with the blood through this dual-lumen needle, into a catheter tube and then into an array of small tubes with ferromagnetic wires placed between them. The entire array of tubes and wires is immersed in a magnetic field that causes the FMMSs to be deflected toward the wires and collected on the walls of the tubes. The detoxified blood then flows out of this array through another section of the catheter tube, then through the dual-lumen needle and finally back into the body.

The performance of the magnetic separator was evaluated theoretically using a streamline analysis of a relatively simple 2-D model that was solved with the aid of Comsol Multiphysics^{TM}. The effect of several parameters on the ability of this magnetic separator to collect the FMMSs was investigated, including the blood velocity (1 to 20 cm/s), magnetic field strength (0.1 to 2.0 T), wire size (0.125 to 2.0 mm in radii), separator unit size at a fixed ratio of tube to wire diameter of unity, tube length (2.0 to 20 cm), wire material (nickel, SS 430 and wairauite), and FMMS magnetic material (iron, magnetite and weaker magnetite).

The results showed that collection efficiencies (CEs) of the FMMSs of well over 80% could easily be attained under reasonable conditions, provided that the blood velocities were below about 2 cm/s. For example, when using FMMSs 400 nm in diameter and containing 60 wt% magnetite, which were both fixed in this study, CEs of this magnitude were obtained in a magnetic field of 0.5 T using a magnetic separator with 0.5 mm radii wire (at a fixed ratio of tube to wire diameter of close to unity) that was 10 cm in length (same as the tube) and made of SS 430. The results also showed that CEs of the FMMSs of between 30% and 80% could easily be attained at higher velocities, even up to 20 cm/s without compromising the practicability of the magnetic separator design. In this regard, the parametric studied showed that the magnetic separator performance could be improved by reducing the size of the unit with tubes and wires of equal radii, maximizing the applied magnetic field strength up to about 1.5 T, utilizing magnetic materials in both the wires and the FMMSs with the highest magnetizations, and increasing the length of the separator unit while keeping in mind the corresponding detrimental effects on pressure drop and portability. Other variables, such as the size of the FMMSs and their content of magnetic material could both also be increased to increase the performance of the magnetic separator, while keeping in mind the corresponding detrimental effects of capillary tube clogging and associated pressure drop.

Overall, the results of this study delineated the physically realistic conditions that make *ex vivo* blood detoxification possible with the magnetic separator device. The success of this blood detoxification approach relies simultaneously on the development of two technologies:

1) highly effective FMMSs for *in vivo* blood detoxification, and
2) a specially designed magnetic separator that can be used to remove the toxin-loaded FMMSs from the body ex vivo.

To this end, the results of this study, which only dealt with the design of the magnetic separator, are further validated with experimental evidence provided in Part II of this work.

ACKNOWLEDGMENTS

This work was supported by the Defense Advanced Research Program Agency-Defense Science Office under contract 8C850, the Department of Energy under contract W-31-109-Eng-38, and the University of Chicago Brain Research and Cancer Research Foundations.

REFERENCES

1. Zhang, R., Hirakawa, K., Seto, D., Soh, N., Nakano, K., Masadome, T., Nagata, K., Sakamoto, K., and Imato, T. (2005) Sequential injection chemiluminescence immunoassay for anionic surfactants using magnetic microbeads immobilized with an antibody. *Talanta*, 68 (2): 231.
2. Kim, K.S. and Park, J.K. (2005) Magnetic force-based multiplexed immunoassay using superparamagnetic nanoparticles in microfluidic channel. *Lab. Chip.*, 5 (6): 657.
3. Soh, N., Nishiyama, H., Asano, Y., Imato, T., Masadome, T., and Kurokawa, Y. (2004) Chemiluminescence sequential injection immunoassay for vitellogenin using magnetic microbeads. *Talanta*, 64 (5): 1160.
4. Jain, K.K. (2003) Nanodiagnostics: application of nanotechnology in molecular diagnostics. *Expert Rev. Mol. Diagn.*, 3 (2): 153.
5. Chosy, E.J., Nakamura, M., Melnik, K., Comella, K., Lasky, L.C., Zborowski, M., and Chalmers, J.J. (2003) Characterization of antibody binding to three cancer-related antigens using flow cytometry and cell tracking velocimetry. *Biotech. and Bioeng.*, 82 (3): 340.
6. Cabioglu, N., Igci, A., Yildirim, E.O., Aktas, E., Bilgic, S., Yavuz, E., Muslumanoglu, M., Bozfakioglu, Y., Kecer, M., Ozmen, V., and Deniz, G. (2002) An ultrasensitive tumor enriched flow-cytometric assay for detection of isolated tumor cells in bone marrow of patients with breast cancer. *Amer. J. Surgery*, 184 (5): 414.
7. McCloskey, K.E., Zborowski, M., and Chalmers, J.J. (2001) Measurement of CD2 expression levels of IFN-α-treated fibrosarcomas using cell tracking velocimetry. *Cytometry*, 44 (2): 137.

8. Liu, Y., Che, Y., and Li, Y. (2001) Rapid detection of Salmonella typhimurium using immunomagnetic separation and immuno-optical sensing method. *Sensors and Actuators B-Chemical*, 72 (3): 214.
9. Fang, B., Zborowski, M., and Moore, L.R. (1999) Detection of rare MCF-7 breast carcinoma cells from mixtures of human peripheral leukocytes by magnetic deposition analysis. *Cytometry*, 36 (4): 294.
10. Hobley, T.J., Ferre, H., Gomes, C.S.G., Hansen, D.B., Petersen, T.L., Buus, S., and Thomas, O.R.T. (2005) Advances in high-gradient magnetic fishing for downstream and bioprocessing. *J. Biotechnol.*, 118: S56.
11. Gupta, A.K. and Gupta, M. (2005) Synthesis and surface engineering of iron oxide nanoparticles for biomedical applications. *Biomaterials*, 26 (18): 3995.
12. Heebøll-Nielsen, A., Justesen, S.F.L., Hobley, T.J., and Thomas, O.R.T. (2004) Superparamagnetic cation-exchange adsorbents for bioproduct recovery from crude process liquors by high-gradient magnetic fishing. *Sep. Sci. Technol.*, 39 (12): 2891.
13. Leyendeckers, H., Tasanen, K., Bruckner-Tuderman, L., Zillikens, D., Sitaru, C., Schmitz, J., and Hunzelmann, N. (2003) Memory B cells specific for the NC16A domain of the 180 kDa bullous pemphigoid autoantigen can be detected in peripheral blood of bullous pemphigoid patients and induced in vitro to synthesize autoantibodies. *J. Investig. Dermatol.*, 120 (3): 372.
14. Lui, G., Manches, O., Chaperot, L., Ducrot, T., Molens, J.P., Sotto, J.J., Bensa, J.C., and Plumas, J. (2004) Preparation of purified lymphoma cells suitable for therapy. *Cytother*, 6 (3): 235.
15. Raghavarao, K.S., Dueser, M., and Todd, P. (2000) Multistage magnetic and electrophoretic extraction of cells, particles and macromolecules. *Adv. Biochem. Eng/Biotech.*, 68: 139.
16. Che, Y.H., Li, Y., Slavik, M., and Paul, D. (2000) Rapid detection of Salmonella Typhimurium in chicken carcass wash water using an immunoelectrochemical method. *J. Food. Pro.*, 63 (8): 1043.
17. Levine, B.L., Cotte, J., Small, C.C., Carroll, R.G., Riley, J.L., Bernstein, W.B., Van Epps, D.E., Hardwick, R.A., and June, C.H. (1998) Large-scale production of CD4+ T cells from HIV-1-infected donors after CD3/CD28 costimulation. *J. Hematother*, 7 (5): 437.
18. Nakayasu, C., Yoshitomi, T., Oyamatsu, T., Okamoto, N., and Ikeda, Y. (1997) Separation of carp (Cyprinus carpio L.) thrombocytes by using a monoclonal antibody, and their aggregation by collagen. *Vet Immunol Immunopathol*, 57 (3–4): 337.
19. Roots-Weiss, A., Papadimitriou, C., Serve, H., Hoppe, B., Koenigsmann, M., Reufi, B., Oberberg, D., Thiel, E., and Berdel, W.E. (1997) The efficiency of tumor cell purging using immunomagnetic $CD34^{+}$ cell separation systems. *Bone Marrow Transpl.*, 19 (12): 1239.
20. Richards, A.J., Roath, O.S., Smith, R.J., and Watson, J.H. (1996) High purity, recovery, and selection of human blood cells with a novel high gradient magnetic separator. *J. Hematother Stem Cell Res.*, 5 (4): 415.
21. Zborowski, M., Sun, L., Moore, L.R., and Chalmers, J.J. (1999) Rapid cell isolation by magnetic flow sorting for applications in tissue engineering. *ASAIO J.*, 45 (3): 127.
22. Sun, L., Zborowski, M., Moore, L.R., and Chalmers, J.J. (1998) Continuous, flow-through immunomagnetic cell sorting in a quadrupole field. *Cytometry*, 33 (4): 469.

23. Ito, A., Shinkai, M., Honda, H., and Kobayashi, T. (2005) Medical application of functionalized magnetic nanoparticles. *J. Biosci. Bioeng.*, 100 (1): 1.
24. Ogiue-Ikeda, M., Sato, Y., and Ueno, S. (2004) Destruction of targeted cancer cells using magnetizable beads and pulsed magnetic forces. *IEEE Trans Magn.*, 40 (4 II): 3018.
25. Ito, A., Kuga, Y., Honda, H., Kikkawa, H., Horiuchi, A., Watanabe, Y., and Kobayashi, T. (2004) Magnetite nanoparticle-loaded anti-HER2 immunoliposomes for combination of antibody therapy with hyperthermia. *Cancer Lett.*, 212 (2): 167.
26. Sonvico, F., Dubernet, C., Colombo, P., and Couvreur, P. (2005) Metallic colloid nanotechnology, applications in diagnosis and therapeutics. *Curr. Pharmaceut Des.*, 11 (16): 2091.
27. Odabasj, M., Özkayar, N., Özkara, S., Ünal, S., and Denizli, A. (2005) Pathogenic antibody removal using magnetically stabilized fluidized bed. *J. Chromat B-Analyt Technol. Biomed. Life Sci.*, 826 (1–2): 50.
28. Odabasi, M. and Denizli, A. (2004) Cibacron blue F3GA incorporated magnetic poly(2-hydroxyethyl methacrylate) beads for lysozyme adsorption. *J. Appl. Polymer Sci.*, 93 (5): 719.
29. Rosengart, A.J. and Kaminski, M.D. (2005) *Nanofabrication Towards Biomedical Applications*; Kumar, S.S.S.R., Hormers, J., and Leuschner, C. (eds.); WILEY-VCH Verlag GmbH & Co. KgaA: Weinheim.
30. Armed Forces Radiobiology Research Institute (AFFRI), in *Medical Management of Radiological Casualties Handbook* edited by Bethesda, M.D. (Armed Forces Radiobiology Research Institute; 1999), p34.
31. National Council on Radiation Protection and Measurements (NCRP). (1980) Management of persons accidentally contaminated with radionucluides. *NCRP Report*, 65: 20.
32. National Council on Radiation Protection and Measurements (NCRP). (2001) Management of terrorist events involving radioactive material. *NCRP Report*, 138: 27.
33. Hoffmann, C., Franzreb, M., and Holl, W.H. (2002) A novel high-gradient magnetic separator (HGMS) design for biotech applications. *IEEE T Appl. Supercond.*, 12 (1): 963.
34. Šafařík, I., Mucha, P., Pechoč, J., Stoklasa, J., and Šafaříková, M. (2001) Separation of magnetic affinity biopolymer adsorbents in a Davis tube magnetic separator. *Biotechnol. Lett.*, 23 (11): 851.
35. Miltenyi, S., Muller, W., Weichel, W., and Radbruch, A. (1990) High gradient magnetic cell separation with MACS. *Cytometry*, 11 (2): 231.
36. Kemshead, J.T., Heath, L., and Gibson, F.M. (1986) Magnetic microspheres and monoclonal antibodies for the depletion of neuroblastoma cells from bone marrow: Experiences, improvements and observations. *Br. J. Cancer*, 54 (5): 771.
37. Rembaum, A., Yen, R.C.K., Kempner, D.H., and Ugelstad, J. (1982) Cell labeling and magnetic separation by means of immunoreagents based on polyacrolein microspheres. *J. Immunolog Methods*, 52 (3): 341.
38. Augusto, P.A., Augusto, P., and Castelo-Grande, T. (2004) Magnetic shielding: Alication to a new magnetic separator and classifier. *J. Magn Magn Mater*, 272 (3): 2296.
39. Karapinar, N. (2003) Magnetic separation of ferrihydrite from wastewater by magnetic seeding and high-gradient magnetic separation. *Int J Miner Process*, 71 (1–4): 45.

40. Newns, A. and Pascoe, R.D. (2002) Influence of path length and slurry velocity on the removal of iron from kaolin using a high gradient magnetic separator. *Miner Eng.*, 15: 465.
41. Nedelcu, S. and Watson, J.H.P. (2002) Magnetic separator with transversally magnetised disk permanent magnets. *Miner Eng.*, 15 (6): 355.
42. Rayner, J.G. and Napier-Munn, T.J. (2000) Mechanism of magnetics capture in the wet drum magnetic separator. *Miner Eng.*, 13 (3): 277.
43. Xiong, D., Liu, S., and Chen, J. (1998) New technology of pulsating high gradient magnetic separation. *Int. J. Miner Process.*, 54 (2): 111.
44. Lin, D., Leroux, M., and Finch, J.A. (1995) Batch magnetohydrostatic separations with a modified Frantz separator. *Miner Eng.*, 8 (3): 283.
45. Inglis, D.W., Riehn, R., Sturm, J.C., and Austin, R.H. (2006) Microfluidic high gradient magnetic cell separation. *J. Appl. Phys.*, 99: 08K101.
46. Smistrup, K., Lund-Olsen, T., and Hansen, M.F. (2006) Microfluidic magnetic separator using an array of soft magnetic elements. *J. Appl. Phys.*, 99 (8): 08P102.
47. Gijs, M.A.M. (2004) Magnetic bead handling on-chip: New opportunities for analytical applications. *Microfluid Nanofluid*, 1 (1): 22.
48. Deng, T., Prentiss, M., and Whitesides, G.M. (2002) Fabrication of magnetic microfiltration systems using soft lithography. *Appl. Phys. Lett.*, 80 (3): 461.
49. Grano, V., Diano, N., Portaccio, M., Bencivenga, U., De Maio, A., De Santo, N., Perna, A., Salamino, F., and Mita, D.G. (2002) The α_1-antitrypsin/elastase complex as an experimental model for hemodialysis in acute catabolic renal failure, extracorporeal blood circulation and cardiocirculatory bypass. *Int. J. Artif Organs*, 25 (4): 297.
50. Yang, M.C. and Lin, C.C. (2000) In vitro characterization of the occurrence of hemolysis during extracorporeal blood circulation using a mini hemodialyzer. *ASAIO J.*, 46 (3): 293.
51. Swartz, R.D., Somermeyer, M.G., and Hsu, C.H. (1982) Preservation of plasma volume during hemodialysis depends on dialysate osmolality. *Am. J. Nephrol.*, 2 (4): 189.
52. Ritter, J.A., Ebner, A.D., Daniel, K.D., and Stewart, K.L. (2004) Application of high gradient magnetic separation principles to magnetic drug targeting. *J. Magn. Magn. Mater.*, 280 (2–3): 184.
53. Chen, H., Ebner, A.D., Rosengart, A.J., Kaminski, M.D., and Ritter, J.A. (2005) Analysis of magnetic drug carrier particle capture by a magnetizable intravascular stent - 2: parametric study with multi-wire two-dimensional model. *J. Magn Magn Mater*, 293 (1): 616.
54. Gerber, R. (1994) Magnetic Separation. In *Applied Magnetism*; Gerber, R., Wright, C.D., and Asti, G. (eds.); Kluwer Academic Publishers: Dordrecht.
55. Bird, R.B., Stewart, W.E., and Lightfoot, E.N. (2002) *Transport Phenomena*, 2nd Edition; Wiley: New York.